Amphiphilic acids as co-adsorbents of metal-free organic dyes for the efficient sensitization of nanostructured photoelectrode

ARTICLE *in* RSC ADVANCES · NOVEMBER 2012

Impact Factor: 3.84 · DOI: 10.1039/C2RA22121G

RSC Advances

Dynamic Article Links

Cite this: *RSC Advances*, 2012, **2**, 11836–11842

www.rsc.org/advances

PAPER

Amphiphilic acids as co-adsorbents of metal-free organic dyes for the efficient sensitization of nanostructured photoelectrode

Constance Magne,[ab] Mathieu Urien,[b] Ilaria Ciofini,[a] Tugba Tugsuz[a] and Thierry Pauporté*[a]

Received 11th September 2012, Accepted 3rd October 2012
DOI: 10.1039/c2ra22121g

Photoelectrode sensitization is an important step of metal-free organic dye-sensitized solar cell (DSSC) preparation. We describe an easy and flexible means for improving organic dye content of ZnO electrodes and avoiding the formation of aggregates by the use of amphiphilic fatty acids as co-adsorbents. A series of fatty acids with variable hydrophobic alkyl chain length has been studied and the D149 indoline dye loading and the recombination step have been optimized. The best performances were measured with butyric acid and octanoic acid. Computing and experimental results show that they present an alkyl chain length compatible with the dye molecule size and structure and provide an efficient re-generation of the oxidized dye by iodide. We also demonstrate that they act as efficient recombination barriers. Moreover the DSSC durability was markedly improved with octanoic acid compared to solar cells without co-adsorbent or with the common cholic acid co-adsorbent. The carrier lifetime increased upon the aging process irrespective of the co-adsorbant due to the increase of the photoelectrode chemical capacitance.

1. Introduction

Dye-sensitized solar cells (DSSCs) based on nanocrystalline oxide semiconductors have been intensively studied and developed over the past decade due to their high performances and potential low production cost.[1–3] The most typical DSSC consists of a nanoparticle TiO_2 photoelectrode sensitized by a ruthenium bipyridine complex and a platinum counter-electrode separated by an iodide-triiodide (I^-/I_3^-) liquid electrolyte.[4] However, in recent years, metal-free organic photosensitizers such as indoline dyes have proved to be highly efficient for the photoelectrode sensitization combined with a good stability.[5–8] Moreover, the wide bandgap TiO_2 layer can be replaced by zinc oxide which has recently emerged as a promising alternative semiconductor material with marked performance improvements of ZnO-based DSSCs achieved during the last few years.[9–15]

The use of additive co-adsorbents is a key point for the preparation of DSSC with high performances.[16–21] They can be added to the electrolyte of the solar cell as done with *tert*-butyl pyridine (TBP) or guanidinium thiocyanate.[16] They are also used to a large extent during the sensitization step as a co-adsorbent of the dye.[17–21] In their pioneering work, Kay and Grätzel[17] found that when cholic acid derivatives were coadsorbed with the dye in DSSCs based on porphyrin-derived photosensitizers, both the photocurrent and the photovoltage of the devices were improved. Since then, chenodeoxycholic acid has been largely employed as a co-adsorbent to improve the efficiency of TiO_2-based organic dye solar cells because the organic D-Π-A push–pull photosensitizers have the tendency to aggregate upon the sensitization step.[19,20] Metal-free indoline organic compounds are among the best dyes for the preparation of ZnO DSSCs with high performances.[12–14,21–23] We have demonstrated elsewhere the deleterious effect of TBP electrolyte additive on indoline sensitized ZnO cell because this compound desorbs the photosensitizer.[24] On the contrary, cholic acid has been shown to markedly improve the performance of indoline dye-sensitized ZnO-devices [21] and has been used in the recent literature on the topic.[15,21]

The choice of chenodeoxycholic acid or cholic acid as dye co-adsorbant in many works is somehow puzzling since these compounds have a rather large steric hindrance and a complicated chemical formula, ($C_{24}H_{40}O_4$) and ($C_{24}H_{40}O_5$) respectively. Therefore, they could be far from being the optimal species. In the present study we have investigated their replacement by saturated fatty acids. These amphiphilic molecules combine cheapness with easy use and molecular tailoring. Moreover, Pauporté *et al.*[25,26] have shown that they can easily form a self-assembled monolayer on the ZnO surface without oxide morphological change. The molecules are attached by their carboxylic acid group with their hydrophobic alkyl chains, oriented in the outer part of the layer, that act as a hydrophobic barrier, highly efficient against water. By studying a series of fatty acids with variable alkyl chain lengths, we show here that higher performances are obtained with rather short fatty acids such as butyric ($C_4H_8O_2$) or octanoic ($C_8H_{16}O_2$) acids compared

[a]*Laboratoire d'Electrochimie, chimie des Interfaces et Modélisation pour l'Energie, UMR-CNRS 7575, Chimie-Paristech, 11 rue P. et M. Curie, 75231 Paris cedex 05, France. E-mail: thierry-pauporte@chimie-paristech.fr; Fax: (33)1 44 27 67 50; Tel: (33)1 55 62 63 83*
[b]*Saint-Gobain Recherche, 39 quai Lucien Lefranc, 93303 Aubervilliers Cedex, France*

to cholic acid. These compounds prevent the dye aggregation and increase the dye loading. Moreover, preliminary results show that, due to the hydrophobic character of the fatty acid alkyl chain, they improve markedly the ZnO device durability and prevent its degradation.

2. Experimental section

2.1 Preparation of the ZnO porous layers

F-doped SnO_2 (FTO) coated glass sheets (TEC-10 from pilkington) were used as the substrate. They were carefully cleaned with detergent, deionized water, acetone and ethanol in an ultrasonic bath for 5 min each. The electrodeposition was carried out in a three-electrode cell. The reference was a saturated calomel electrode (SCE) (with a potential at +0.25V *vs.* NHE) placed in a separate compartment maintained at room temperature. The FTO/glass substrate was fixed to a rotating electrode and used as the working electrode. The rotation speed was set at 300 rpm. The bath temperature was controlled at 70 °C. It contained initially 0.1 M KCl as the supporting electrolyte, 5 mM $ZnCl_2$ and was saturated with molecular oxygen by an intense bubbling. The counter-electrode was a zinc wire. A thin continuous blocking ZnO layer was then produced on the FTO for 10 min with an applied potential of −1.0V *vs.* SCE. The nanoporous second layer was then electrodeposited at the same potential for 20 min after addition of 50 μM EY in the bath.[27,28] Eosin Y incorporated in the film was subsequently removed by soaking in a KOH solution at pH 10.5 overnight.[29] The film thicknesses were measured with a Dektak 6M stylus profiler. Their mean total thickness was about 6 μm.

2.2 Device preparation and characterization

After treatment at 150 °C for 30 min, the porous ZnO films were immersed upon cooling in a sensitizing solution for 15 min. The solution contained 0.5 mM D149 dye (see Fig. 1 inset) in a 1 : 1 volume mixture of acetonitrile/*tert*-butanol.[15] Various acids, listed in Table 1, were tested as co-adsorbent at 1 mM in the sensitization solution. Four different fatty acids with increasing alkyl saturated chains from C4 to C18 were investigated and

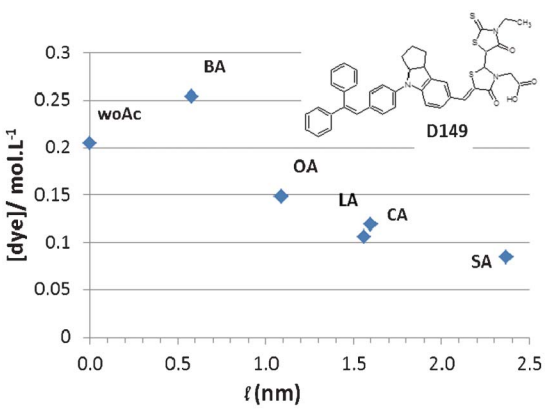

Fig. 1 Dye concentration in the photoanode as a function of the acid co-adsorbent length (ℓ). (woAc: without acid; BA: butyric acid; OA: Octanoic acid; LA: Lauric acid; CA: Cholic acid and SA: stearic acid). The inset is the molecular structure of D149 indoline dye.

Table 1 List of acids studied as co-adsorbent and their molecular lengths calculated by DFT from the bonding-carboxylate oxygen (for comparison, the length of D149 dye is calculated at 21.671 Å)

Name	Formulae	Molar mass (g mol^{-1})	Maximum length (Å)
Butyric acid (BA)	$C_4H_8O_2$	88.1	5.850
Octanoic acid (OA)	$C_8H_{16}O_2$	144.2	10.948
Lauric acid (LA)	$C_{12}H_{24}O_2$	200.3	16.050
Stearic acid (SA)	$C_{18}H_{36}O_2$	284.5	23.705
Cholic acid (CA)	$C_{24}H_{40}O_5$	408.6	15.671

compared to cholic acid. The counter-electrode was prepared using a FTO glass substrate (TEC7, Pilkington) cleaned by ultrasound in acetone and ethanol for 5 min each. They were then treated in a furnace for 30 min at 450 °C to remove organic contaminants. The Pt catalyst was deposited onto the FTO glass by spreading a 10 μL drop of H_2PtCl_6 solution (6 mg Pt in 1 mL ethanol) and subsequent heating at 400 °C for 20 min. This step was repeated once. The two electrodes were sealed with a 60 μm hot melting spacer (Surlyn, DuPont) and the internal space between the two was filled with the electrolyte through a hole drilled in the counter electrode which was subsequently sealed with Surlyn and aluminum foil. The electrolyte composition was 0.05 M I_2 and 0.5 M 1,2-dimethyl-3-propylimidazolium iodide (DMPII) in acetonitrile. For the aging test, for each sensitization condition, more than five devices were prepared, stored under laboratory ambient conditions and followed by characterizations. The sealant was the surlyn film without any other special encapsulation. No electrolyte drying was observed upon our test period.

For the J–V curves, the solar cells were illuminated with a solar simulator (Abet Technology Sun 2000) filtered to AM 1.5G conditions. The illuminated surface was delimited by a black mask with an aperture diameter of 4 mm. The power density was calibrated at 100 mW cm^{-2} by using a silicon solar cell reference. The J–V curves were recorded by a Keithley 2400 digital sourcemeter, using a 0.01 V s^{-1} voltage sweep rate. The incident-photon-to-electron-conversion efficiency (IPCE) curves were measured at the short circuit with a home-made system using a Jobin-Yvon monochromator and a calibrated Newport power-meter. The impedance spectra were measured at the open circuit voltage, V_{oc}, under 1 sun AM 1.5 illumination by a Solartron FRA1255 coupled with a PAR273 potentiostat. The AC signal was 10 mV and the frequency range was 100 kHz-1 Hz. The spectra were fitted and analysed using the Zview modeling software (Scribner). The D149 concentration in the photoelectrodes was measured by dye desorption in 4 mL of dimethylformamide (DMF). The solution dye concentration was subsequently titrated by spectrophotometry using 72 350 L mol^{-1} cm^{-1} at 530 nm as the molar extinction coefficient. The dye concentration was then calculated using the measured film thickness.

Density functional theory (DFT) calculations were performed using the Gaussian09 program.[30] The Zn[1010] surface was modeled by a large hydrogen-saturated cluster (530 atoms) obtained from the optimized periodic structure which has been previously used to simulate the UV-Vis spectra of an organic dye on surface.[31] Fatty acids were adsorbed (and D149) on a fixed surface fixing the Zn to O (carboxylate) distance to 1.99 A and

all the other degrees of freedom were left free to relax. The fatty acids (and D149) on the surface were computed by the mean of an ONIOM approach,[32] the organic molecule being treated at B97-D/6-31+G(d)[33] level while the surface was treated at semi-empirical level.[34] Free fatty acids and D149 molecules were also fully optimized as isolated systems at the same level of theory (B97-D/6-31+G(d))). Calculations allowed defining both fatty acids and D149 length as well as inter-fatty acids interaction energies. These latter were computed co-adsorbing three fatty acids on the cluster. From our calculations it seems that all acids with chain length starting from octanoic one displays comparable acid-acid interaction energies and close to the one obtained for cholic acid. Analogously, the computed interaction energy between a D149 dye molecule and two nearby cholic or lauric acid is computed to be fully comparable.

3. Results and discussion

The effects of acid co-adsorbent on the photoelectrode characteristics were first investigated by measuring the D149 dye concentration in the layers. Fig. 1 shows the titration results after full dye desorption in dimethylformamide (DMF), a solvent with a high donor number.[24] Without co-adsorbent, the dye concentration was 0.205 mol L^{-1} after 15 min of sensitization and 0.260 mol L^{-1} after 30 min. We observed that the concentration of dye in the layer was higher in the presence of butyric acid. In Fig. 1 the dye concentration is reported as a function of the co-adsorbent molecular length (ℓ) calculated by DFT (see Table 1) and decreases with this parameter. We also note that the dye concentration was close for cholic acid and lauric acid which have a similar molecular length.

The cell J–V curves under full sun are presented in Fig. 2a and the solar cell characteristics are listed in Table 2. The important result is that the devices prepared with the shortest fatty acids, namely butyric acid and octanoic acid, gave rise to the best performances (4.73% for an optimized D149/octanoic acid DSSC (See Table 2)). They are characterized by high short circuit current (J_{sc}) and fill factors (FF). Cholic acid, which is classically used as the D149 co-adsorbent, yielded to cells with higher open circuit voltage (V_{oc}) but had lower overall performances. The dark current (J_{dark}) is reported in Fig. 2b. High dark current was measured in the absence of co-adsorbent. This parameter was reduced in the presence of acid species that adsorb on the oxide surface and reduce the recombination between electrons in ZnO and I_3^-. We also observe that for the fatty acid series, J_{dark} decreased with the molecular size. The lowest dark current was measured with cholic acid which yielded the highest cell V_{oc} (Table 2).

J_{sc} is plotted as a function of dye concentration in Fig. 3a. We observe that the dot without acid co-adsorbent is below the trend of the devices prepared with acid co-adsorbent. This is due to the presence of aggregates. J_{sc} is similar to that of solar cells sensitized with cholic or lauric acid that have half its concentration of dye. We can suppose that, in the absence of co-adsorbent, half of the dye is not connected to ZnO and cannot act efficiently for the charge injection in the semiconductor. For the devices prepared with an acid co-adsorbent, J_{sc} increased with the concentration of dye and reached a plateau above 0.15 mol L^{-1} because the sunlight harvesting increased with the dye loading. We can also note that the J_{sc} of stearic acid is very low (Fig. 3a).

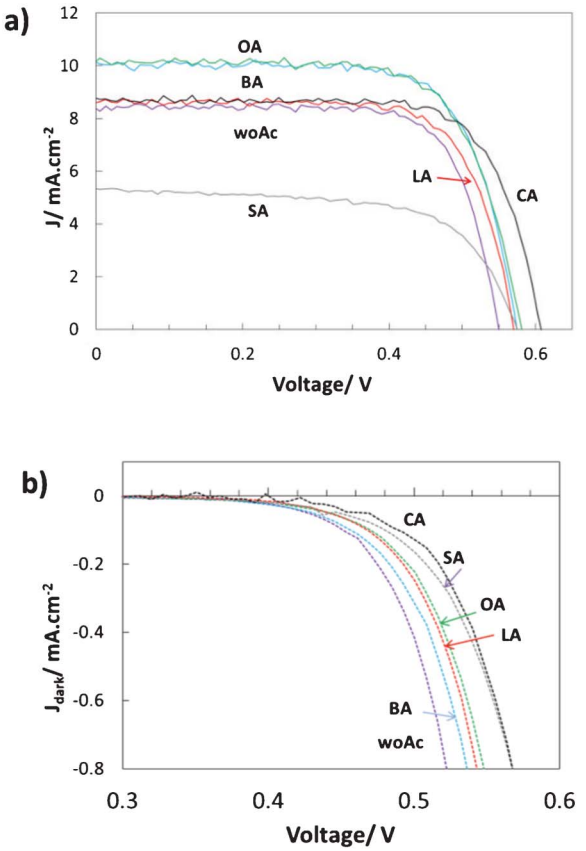

Fig. 2 (a) Photocurrent–Voltage curves under AM1.5G illumination 100 mW cm^{-2} and (b) Dark current–voltage (J–V) curves for D149 solar cells sensitized without and with various acid co-adsorbents.

In that case the problem is not only the light havesting but also the dye regeneration by I^-. Fig. 4 shows that stearic acid co-adsorbent is much longer than the indoline dye. Therefore the donor group of the photosensitizer is partly masked by the akyl chains and the regeneration of the oxidized dye by I_3^- is difficult and can limit the device photocurrent.

In Fig. 4 we observe that the same effect could also occur in the case of lauric acid but to a much less extent, whereas the butyric and the octanoic acids cover efficiently the surface, to protect the dye carboxylic acid anchoring group and do not limit the access of the dye donor group[22] to I_3^-.

In Fig. 3b, the IPCE curve of a DSSC without co-adsorbent is compared to those of solar cells prepared with cholic acid and octanoic acid. Very high solar energy conversion efficiency were found between 480 and 620 nm with the presence of a plateau over this wavelength range. Values higher than 70% were obtained. The presence of acid co-adsorbent increased significantly the conversion efficiency because it avoided the formation of dye aggregates and the best result was found for octanoic acid which yielded to the optimized dye loading. The curves were integrated between 380 and 700 nm and the calculated J_{sc} presented in Table 2 fit well with the measured values.

To better understand the effect of the co-adsorbent on the device functioning, we have performed impedance spectroscopy measurements under calibrated 1 sun illumination at the V_{oc}. The spectra are presented in Fig. 5a and 5b. The high frequency

Table 2 Photoelectrode dye loadings and DSSC parameters under 100 mW cm^{-2}, AM 1.5G filtered illumination

Acid co-adsorbent	Dye concentration (mol L^{-1})	V_{oc} (V)	J_{sc} (mA cm^{-2})	FF (%)	η (%)	τ_n (ms)	DOS (10^{18} cm^{-3})	$J_{sc}^{IPCE\ a}$ (mA cm^{-2})
Without	0.205	0.55	8.4	75	3.46	4	3.7	8.3
Butyric	0.254	0.58	10.1	73	4.22	13	14.0	—
Octanoic	0.149	0.58 (0.56)[b]	10.2 (12.1)[b]	71 (70)[b]	4.18 (4.73)[b]	9	8.9	9.7
Lauric	0.119	0.57	8.6	74	3.61	10	9.1	—
Stearic	0.085	0.58	5.3	64	1.97	7	3.7	—
Cholic	0.106	0.61	8.8	73	3.89	9	8.6	8.7

[a] Calculated by integration of the IPCE curves between 380 and 700 nm. [b] Best cell.

semicircle is due to the redox reaction of I^-/I_3^- at the platinum counter-electrode. The corresponding resistance is small and demonstrates the fast tri-iodide regeneration at the counter-electrode. The low-frequency semicircle is related to the charge transfer (recombination) at the photosensitized-oxide/electrolyte interface. In the case of nanoporous electrodeposited ZnO photoelectrodes, we have never observed at the V_{oc} the transmission line feature in the mid-frequency range which is commonly attributed to electron diffusion transport in the semiconductor oxide.[4,35–37] This is due to the good conducting properties in the oxide material. For this reason, it was not possible to extract reliable transport resistance values from the spectra and we have limited our study to the recombination behavior at the photoelectrodes. The electrical circuit used to fit the data is presented in Fig. 5c. The low frequency part of the spectra was fitted with a R_{ct}//CPE_{ct} circuit, where R_{ct} is the charge transfer resistance. The CPE electrical element (with an impedance written $Z_{CPE} = 1/Q(j\omega)^a$) was used to take into account the dispersion of capacitance. The capacitance, noted C_μ, was deduced from the resistances and CPE parameters according to:[38,39]

$$C_\mu = \left[Q_{ct} \left(\frac{1}{R_s + R_{Pt}} + \frac{1}{R_{ct}} \right)^{a-1} \right]^{1/a} \quad (1)$$

with R_s the series resistance mainly due to the electrical contacts and ohmic drops in the FTO layers. If the semiconductor is nanostructured and not highly doped, no space charge is built in the semiconductor. The capacitance is due to the density of electronic state (DOS) and it is termed ''chemical'' capacitance. The states classically show more or less an exponential distribution in the bandgap, below the bottom of the conduction band. The DOS parameter was calculated using the formalism proposed by O'Regan *et al.*:[40]

$$DOS = \frac{C_\mu}{qAL(1-p)} \quad (2)$$

with q the electron charge, A the geometric area of the DSSC and p the film porosity (determined at about 0.6 for electrodeposited nanoporous ZnO films).[28]

In Fig. 5d is displayed the DOS value as a function of the dye concentration. Without co-adsorbent the DOS is low due to the presence of dye aggregate and inefficient electron injection. For the solar cells with co-adsorbent, the DOS value increases continuously with the dye concentration: the better electron

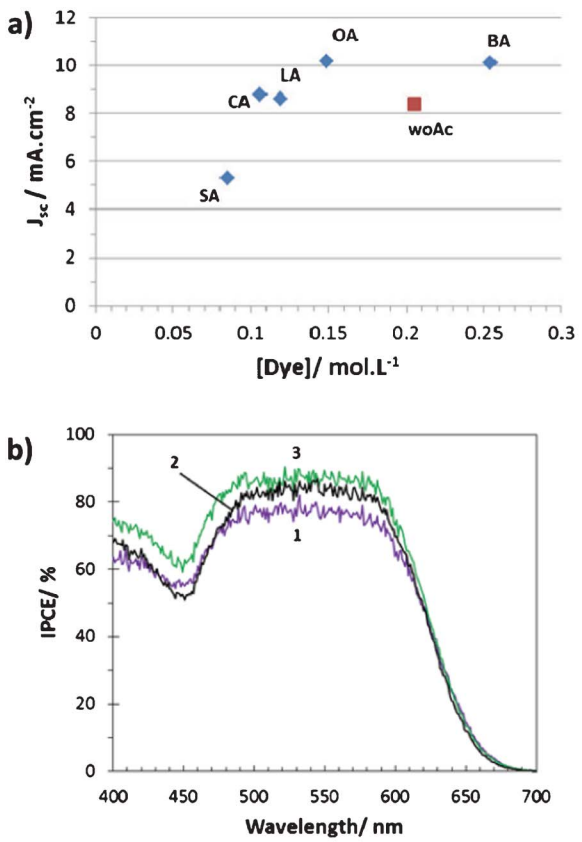

Fig. 3 (a) J_{sc} *versus* dye loading plot; (b) photocurrent action spectra of solar cells sensitized (1) without acid, (2) with cholic acid and (3) with octanoic acid.

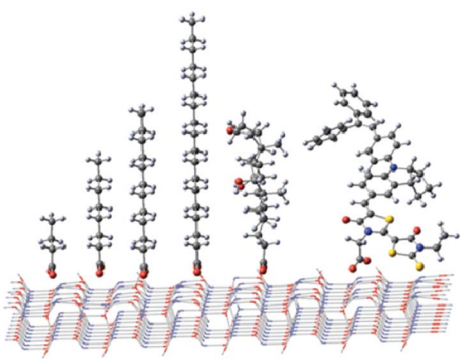

Fig. 4 Schematic view of (from left to right): butyric acid, octanoic acid, lauric acid, stearic acid, cholic acid and D149 dye adsorbed on the saturated ZnO cluster used to simulate the (10-10) plane of ZnO.

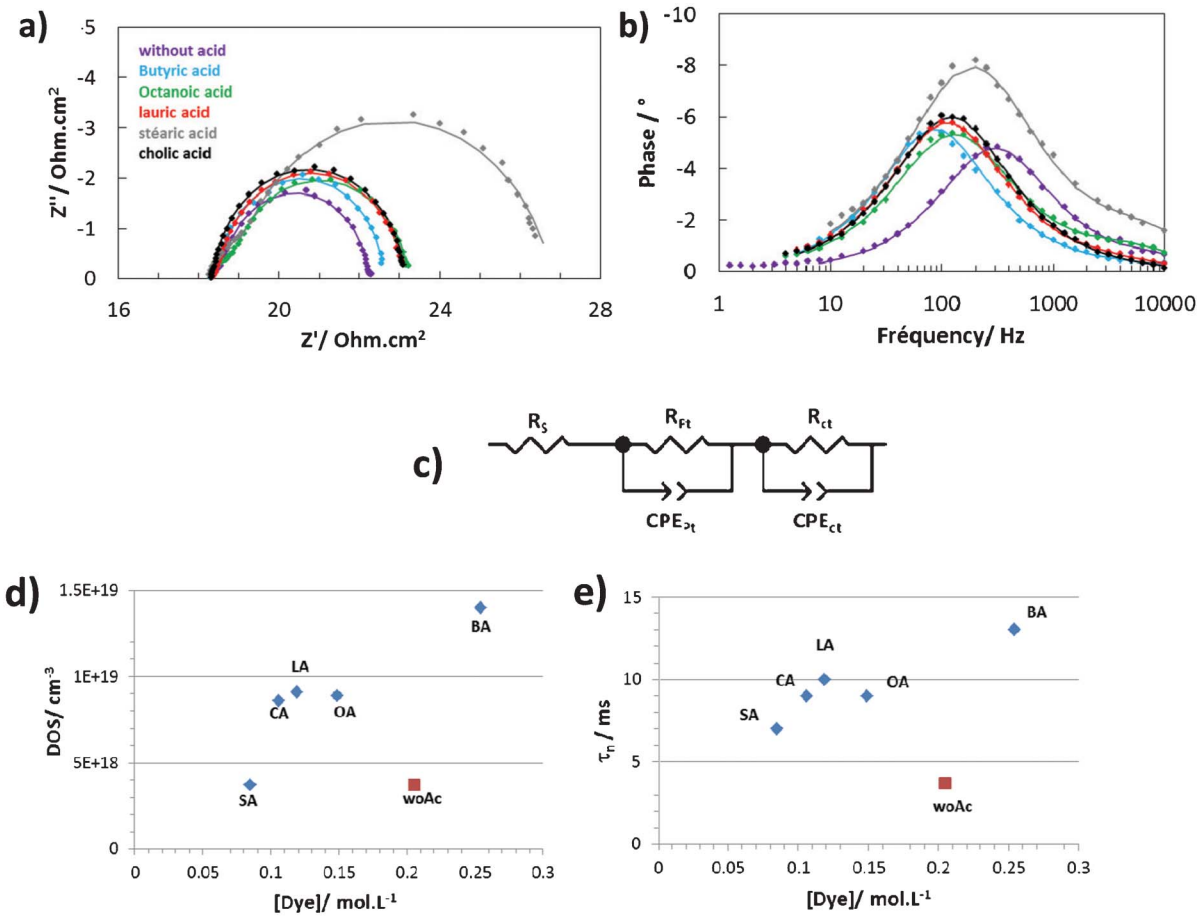

Fig. 5 Impedance spectra of DSSCs prepared with and without co-adsorbent (a) Nyquist plot; (b) Phase *versus* frequency plot. (c) Electrical circuit used to fit the data (the fits are the solid lines in (a) and (b)). (d) DOS as a function of the dye photoelectrode concentration. (e) Electron lifetime as a function of the dye photoelectrode concentration.

injection gives rise to higher filling of the states localized below the conduction band edge.

The lifetime of the electrons in the photoelectrodes, τ_n, was then determined by:

$$\tau_n = 2\pi R_{ct} C_\mu \quad (3)$$

In Fig. 5e, τ_n is reported as a function of the dye concentration. The electron lifetime is increased in the presence of co-adsorbent. These molecules fill the space of ZnO surface uncoverved by the indoline dye and act as a barrier between the semiconductor and the electrolyte. Therefore they reduce the recombination of electrons localized near the conduction band and the tri-iodide ions and increases τ_n. Except for butyric acids, the other co-adsorbants give similar τ_n. The fact that cholic acid gives rise to higher cell V_{oc} (Table 2) suggests that it is not due to lower recombinations but to a higher conduction band-edge position.

The stability of ZnO based DSSC has been poorly investigated in the literature and to the best of our knowledge, no optimized systems have been reported. Here, to test basically the effect of sensitization condition on stability, several devices were sealed by a Surlyn film without any other special care and were followed by J–V and impedance characterizations. They were stored under ambient conditions and their performances and impedance spectra were measured periodically. In Fig. 6 is reported the mean evolution of D149/octanoic acid DSSCs. Slow decrease of FF and V_{oc} were found whereas J_{sc} slightly increased. The device overall efficiency showed an excellent photostability when submitted to a long storage with an initial efficiency at 4.53% and a final one at 4.43%. The variations of R_{ct} and C_μ upon aging are shown in Fig. 6c. The slight initial increases of V_{oc} (Fig. 6b) can be related to the increase of R_{ct}. This parameter was then slightly decreased and no significant degradation of the recombination reaction was observed. A significant concomitant increase of C_μ was found upon aging. In Fig. 7a aging of devices without co-adsorbent, with cholic acid and octanoic acid are compared. Without co-adsorbent, the overall efficiency deacreased by 25% after more than 125 days. It was only 8.8% in the case of cholic acid and less than 2% with octanoic acid. The study demonstrates that the solar cells prepared with the best fatty acid were highly stable without significant performance deterioration after 125 days. The main degradation reaction of indoline dyes in DSSC has been identified by Tanaka *et al.*[8] They showed that oxidizing species give rise to the decarboxylation of indoline and to the dye detachment. Modeling of the fatty acid adsorption on the ZnO surface shows that fatty acids are bound to the oxide surface by means of the carboxylic acid group and

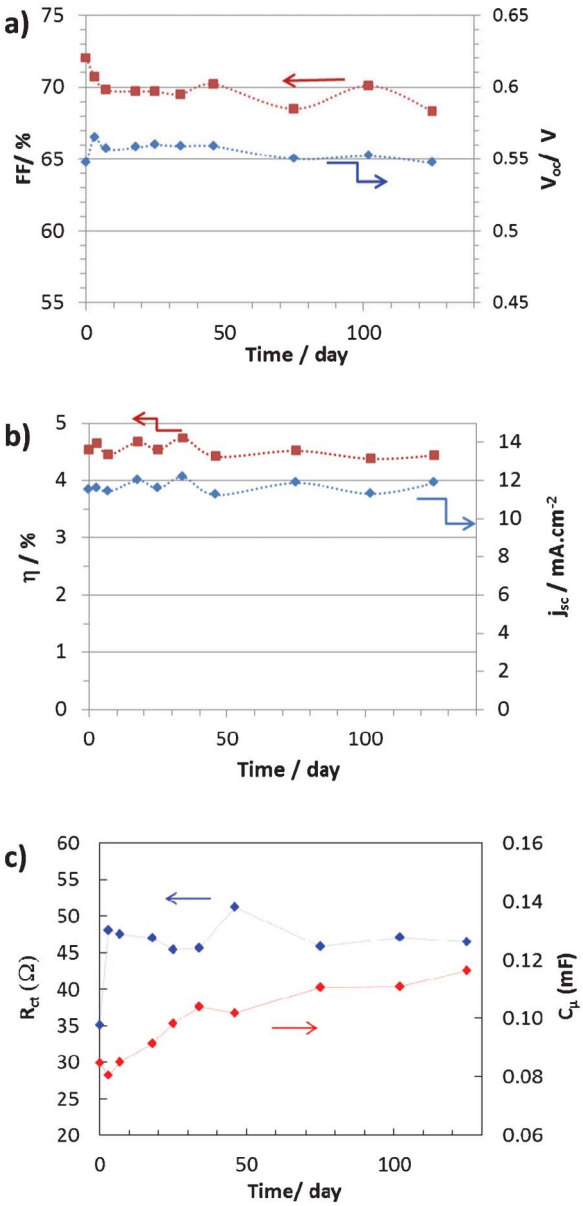

Fig. 6 D149/octanoic acid DSSC parameters variation with storage time. (a) FF and V_{oc}; (b) J_{sc} and η; (c) R_{ct} and C_μ.

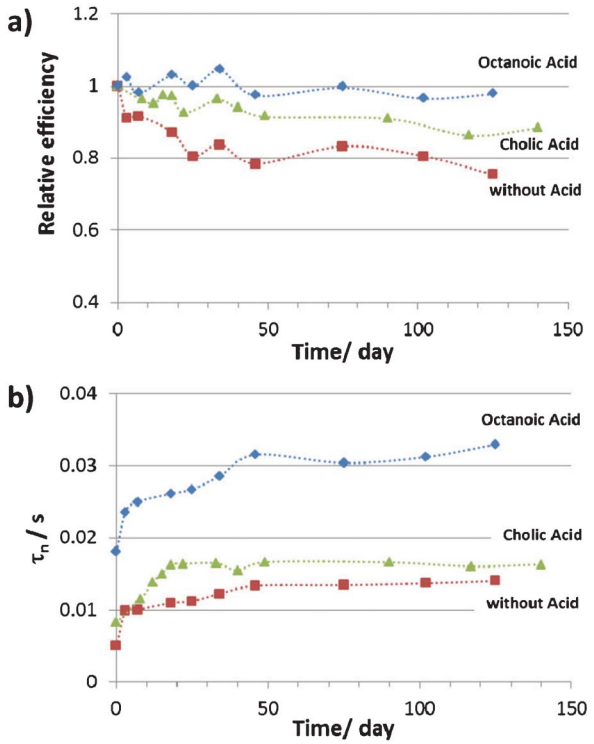

Fig. 7 (a) Relative efficiency ($\eta/\eta_{initial}$) and (b) electron lifetime evolution upon storage under ambient conditions.

that the hydrophobic alkyl chain is localized perpendicular to the surface. The alkyl chain acts as an efficient barrier between the electrolyte and the zinc oxide. We can then suppose that this hydrophobic barrier prevents the diffusion of water traces and oxidizing molecules towards the oxide surface and protect the anchoring group of the dye. We can note that the classical approach to prepare robust DSSCs is to use amphiphilic dyes with grafted long alkyl chains (such as Z907 or K19 dyes).[41,42] Our approach was different here. The amphiphilic molecule was the co-adsorbent which can be easily combined with any highly efficient dyes without modification to yield robust devices. The high flexibility of the system is very promising.

From the impedance spectra, the evolution of τ_n, defined by eqn (3), was followed with time as presented in Fig. 7b. For the DSSCs without and with co-adsorbent, an increase of τ_n during the first 45 days was found and then this parameter remained virtually stable. We can note that an increase was also found for the less stable devices, prepared without co-adsorbent. The D149/octanoic acid devices kept the highest τ_n over the aging process and their values stabilized above 30 ms. τ_n of ZnO solar cell are about ten times shorter than those we measured at the V_{oc} for TiO_2 nanoparticle-based DSSCs.[4] The τ_n increase is due to the rises of C_μ (Fig. 6c) wheras R_{ct} is virtually stable, therefore our results and eqn (2) suggest a filling of the states localized in the bandgap upon aging by a doping process that could be hydrogen insertion.[43,44]

4. Conclusions

We have described a very easy and flexible means for the improvement of metal-free dye sensitized ZnO solar cells and we believe that the process could be extended to other DSSC dye/oxide systems. By studying a series of fatty acids with variable alkyl chain length as co-adsorbent of the sensitizer, the dye loading and the recombination step have been optimized. The best efficiencies were measured with butyric acid and octanoic acid. These acids presented an alkyl chain length compatible with the dye molecule size and structure and provided an efficient regeneration of the oxidized dye by iodide. Moreover, they acted as efficient recombination barriers. The DSSC durability was shown higher with octanoic acid compared to without co-adsorbent or with the common cholic acid co-adsorbent. The carrier lifetime increased with aging due to a filling of the sub-conduction band edge states upon aging. Hydrogen insertion is suggested to be at the origin of the DOS change.

Acknowledgements

The authors are grateful to Dr H. Miura (Chemicrea Inc., Japan) for providing them with the indoline dye.

References

1 B. O'Regan and M. Grätzel, *Nature*, 1991, **353**, 737.
2 K. Kalyanasundaram, Ed., *Dye-sensitized solar cells*, EPFL press, Lausanne, 2010.
3 A. Hagfeldt, G. Boschloo, L. Sun, L. Kloo and H. Pettersson, *Chem. Rev.*, 2010, **110**, 6595.
4 C. Magne, F. Dufour, F. Labat, G. Lancel, O. Durupthy, S. Cassaignon and T. Pauporté, *J. Photochem. Photobiol., A*, 2012, **232**, 22.
5 H. Choi, I. Raabe, D. Kim, F. Teocoli, C. Kim, K. Song, J. H. Yum, J. Ko, M. K. Nazeeruddin and M. Grätzel, *Chem.–Eur. J.*, 2010, **16**, 1193.
6 J. Tang, J. L. Hua, W. J. Wu, J. Li, Z. G. Jin, Y. T. Long and H. Tian, *Energy Environ. Sci.*, 2010, **3**, 1736.
7 M. K. R. Fischer, S. Wenger, M. K. Wang, A. Mishra, S. M. Zakeeruddin, M. Grätzel and P. Bauerle, *Chem. Mater.*, 2010, **22**, 1836.
8 H. Tanaka, A. Takeichi, K. Higuchi, T. Motohiro, M. Takata, N. Hirota, J. Nakajima and T. Toyoda, *Sol. Energy Mater. Sol. Cells*, 2009, **93**, 1143.
9 K. Keis, E. Magnusson, H. Lindström, S. E. Lindquist and A. Hagfeldt, *Sol. Energy Mater. Sol. Cells*, 2002, **73**, 51.
10 Q. Zhang, C. S. Dandeneau, X. Zhou and G. Cao, *Adv. Mater.*, 2009, **21**, 4087.
11 Q. Zhang, T. P. Chou, B. Russo, S. A. Jenekhe and G. Cao, *Angew. Chem., Int. Ed.*, 2008, **47**, 2402.
12 T. Yoshida, J. Zhang, D. Komatsu, S. Sawatani, H. Minoura, T. Pauporté, D. Lincot, T. Oekermann, D. Schlettwein, H. Tada, D. Wörhle, K. Funabiki, M. Matsui, H. Miura and H. Yanagi, *Adv. Funct. Mater.*, 2009, **19**, 17.
13 V. M. Guérin, C. Magne, T. Pauporté, T. Le Bahers and J. Rathousky, *ACS Appl. Mater. Interfaces*, 2010, **2**, 3677.
14 H. M. Cheng and W. F. Hsieh, *Nanotechnology*, 2010, **21**, 485202.
15 V. M. Guérin and T. Pauporté, *Energy Environ. Sci.*, 2011, **4**, 2971.
16 S. Ito, T. N. Murakami, P. Comte, P. Liska, C. Grätzel, K. Nazeeruddin and M. Grätzel, *Thin Solid Films*, 2010, **516**, 4613.
17 A. Kay and M. Grätzel, *J. Phys. Chem.*, 1993, **97**, 6272.
18 P. Wang, S. M. Zakeeruddin, P. Comte, R. Charvet, R. Humphry-Baker and M. Grätzel, *J. Phys. Chem. B*, 2003, **107**, 14336.
19 K. Hara, Y. Dan-Oh, C. Kasada, Y. Ohga, A. Shinpo, S. Suga, K. Sayama and H. Arakawa, *Langmuir*, 2004, **20**, 4205.
20 Z. S. Wang, Y. Cui, Y. Dan-Oh, C. Kasada, A. Shinpo and K. Hara, *J. Phys. Chem. C*, 2007, **111**, 7224.
21 Y. Sakuragi, X. F. Wang, H. Miura, M. Matsui and T. J. Yoshida, *J. Photochem. Photobiol., A*, 2010, **216**, 1.
22 T. Le Bahers, T. Pauporté, G. Scalmani, C. Adamo and I. Ciofini, *Phys. Chem. Chem. Phys.*, 2009, **11**, 11276.
23 R. Scholin, M. Quintana, E. M. J. Johansson, M. Hahlin, T. Marinado, A. Hagfeldt and H. Rensmo, *J. Phys. Chem. C*, 2011, **115**, 19274.
24 T. Le Bahers, F. Labat, T. Pauporté and I. Ciofini, *Phys. Chem. Chem. Phys.*, 2010, **12**, 14710.
25 C. Badre, T. Pauporté, M. Turmine and D. Lincot, *Nanotechnology*, 2007, **18**, 365705.
26 T. Pauporté, G. Bataille, L. Joulaud and F. J. Vermersch, *J. Phys. Chem. C*, 2010, **114**, 194.
27 T. Pauporté, T. Yoshida, A. Goux and D. Lincot, *J. Electroanal. Chem.*, 2002, **534**, 55.
28 T. Pauporté and J. Rathousky, *J. Phys. Chem. C*, 2007, **111**, 7639.
29 T. Yoshida, M. Iwaya, H. Ando, T. Oekermann, K. Nonomura, D. Schlettwein, D. Wöhrle and H. Minura, *Chem. Commun.*, 2004, 400.
30 Gaussian 09, Revision C.1, M. J. Frisch, G. W. Trucks, H. B. Schlegel, G. E. Scuseria, M. A. Robb, J. R. Cheeseman, G. Scalmani, V. Barone, B. Mennucci, G. A. Petersson, H. Nakatsuji, M. Caricato, X. Li, H. P. Hratchian, A. F. Izmaylov, J. Bloino, G. Zheng, J. L. Sonnenberg, M. Hada, M. Ehara, K. Toyota, R. Fukuda, J. Hasegawa, M. Ishida, T. Nakajima, Y. Honda, O. Kitao, H. Nakai, T. Vreven, J. A. Montgomery, Jr., J. E. Peralta, F. Ogliaro, M. Bearpark, J. J. Heyd, E. Brothers, K. N. Kudin, V. N. Staroverov, R. Kobayashi, J. Normand, K. Raghavachari, A. Rendell, J. C. Burant, S. S. Iyengar, J. Tomasi, M. Cossi, N. Rega, J. M. Millam, M. Klene, J. E. Knox, J. B. Cross, V. Bakken, C. Adamo, J. Jaramillo, R. Gomperts, R. E. Stratmann, O. Yazyev, A. J. Austin, R. Cammi, C. Pomelli, J. W. Ochterski, R. L. Martin, K. Morokuma, V. G. Zakrzewski, G. A. Voth, P. Salvador, J. J. Dannenberg, S. Dapprich, A. D. Daniels, Ö. Farkas, J. B. Foresman, J. V. Ortiz, J. Cioslowski, and D. J. FoxGaussian, Inc., Wallingford CT, 2009.
31 T. Le Bahers, F. Labat, T. Pauporté, P. Lainé and I. Ciofini, *J. Am. Chem. Soc.*, 2011, **133**, 8005.
32 S. Dapprich, I. Komáromi, K. S. Byun, K. Morokuma and M. J. Frisch, *THEOCHEM*, 1999, **461–462**, 1–21.
33 S. Grimme, *J. Comput. Chem.*, 2006, **27**, 1787–99.
34 J. J. P. Stewart, *J. Mol. Model.*, 2007, **13**, 1173–213.
35 J. Bisquert, *J. Phys. Chem. B*, 2002, **106**, 325.
36 J. Bisquert and V. S. Vikhrenko, *J. Phys. Chem. B*, 2004, **108**, 2313.
37 Q. Wang, J. E. Moser and M. Grätzel, *J. Phys. Chem. B*, 2005, **109**, 14945.
38 G. J. Brug, A. L. G. Vanden Eeden, M. Sluyters-Rehabach and J. H.Sluyters, *J. Electroanal. Chem.*, 1984, **176**, 275.
39 Th. Pauporté and J. Finne, *J. Appl. Electrochem.*, 2006, **36**, 33.
40 B. O'Regan, J. R. Durrant, P. M. Sommeling and N. J. Bakker, *J. Phys. Chem. C*, 2007, **111**, 14001.
41 M. Grätzel, C. R. Chimie, 2006, **9**, 578.
42 H. Desilvestro, M. Bertoz, S. Tulloch and G. Tulloch, in *Dye-sensitized solar cells*, K. Kalyanasundaram, Ed., p.224–230, EPFL press, Lausanne, 2010.
43 D. G. Thomas and J. J. Lander, *J. Chem. Phys.*, 1956, **25**, 1136.
44 C. G. Van de Walle, *Phys. Rev. Lett.*, 2000, **85**, 1012.

